ELSEVIER

Earth and Planetary Science Letters 152 (1997) 59–73

EPSL

Cosmogenic dating of fluvial terraces, Fremont River, Utah

James L. Repka [a], Robert S. Anderson [a,*], Robert C. Finkel [b]

[a] *Department of Earth Sciences and Institute for Tectonics, University of California, Santa Cruz, CA 95064, USA*

[b] *Geosciences and Environmental Technology Division and Center for Accelerator Mass Spectrometry, Lawrence Livermore National Laboratory, Livermore, CA 94550, USA*

Received 19 March 1997; accepted 25 August 1997

Abstract

Absolute dating of river terraces can yield long-term incision rates, clarify the role of climate in setting times of aggradation and incision, and establish the rates of pedogenic processes. While surface exposure dating using cosmogenic ^{10}Be and ^{26}Al would seem to be an ideal dating method, the surfaces are composed of individual clasts, each with its own complex history of exposure and burial. The stochastic nature of burial depth and hence in nuclide production in these clasts during exhumation and fluvial transport, and during post-depositional stirring, results in great variability in clast nuclide concentrations. We present a method for dealing with the problem of pre-depositional inheritance of cosmogenic nuclides. We generate samples by amalgamating many individual clasts in order to average over their widely different exposure histories. Depth profiles of such amalgamated samples allow us to constrain the mean inheritance, to test for the possible importance of stirring, and to estimate the age of the surface. Working with samples from terraces of the Fremont River, we demonstrate that samples amalgamated from 30 clasts represent well the mean concentration. Depth profiles show the expected shifted exponential concentration profile that we attribute to the sum of uniform mean inheritance and depth-dependent post-depositional nuclide production. That the depth-dependent parts of the profiles are exponential argues against significant post-depositional displacement of clasts within the deposit. Our technique yields ^{10}Be age estimates of 60 ± 9, 102 ± 16 and 151 ± 24 ka for the three highest terraces, corresponding to isotope stages 4, 5d and 6, respectively. The mean inheritance is similar from terrace to terrace and would correspond to an error of ~ 30–40 ka if not taken into account. The inheritance likely reflects primarily the mean exhumation rates in the headwaters, of order 30 m/Ma. © 1997 Elsevier Science B.V.

Keywords: cosmogenic elements; terraces; fluvial features; absolute age

1. Introduction

Strath terraces represent ancient floodplains of a river that is incising into bedrock. They are formed when, after remaining at the same elevation and widening its floodplain for a period of time, a river begins to incise again, abandoning its old flood plain. Accurate dating of strath terrace deposits can constrain the rate of incision of the stream system as well as the timing of the events that control incision rates. This information can be used to determine the response time of a fluvial system to base level lowering or to rock uplift within the drainage basin. River terraces are excellent chronosequence sites for the study of soil profile development (e.g., [3]), clast

* Corresponding author. Fax: +1 408 459 3074. E-mail: jlrpk@bagnold.ucsc.edu

PII S0012-821X(97)00149-0

weathering, and eolian inflation, the rates of which may be constrained by dating the deposits.

Dating fluvial terraces is often difficult, however. If suitable organic remains can be located, ^{14}C may be employed to date material deposited in the most recent of the late Pleistocene climatic cycles. Some terraces sequences have been dated using tephra [3,4], or by correlation with moraines [5,6]. U/Th dating of soil carbonate coatings on subsurface clasts has been employed in some settings (e.g., [3,7]), although this technique suffers from an unknown lag between deposition of the clast and accumulation of the innermost carbonate coating.

While in situ produced cosmogenic radionuclides ^{10}Be, ^{26}Al, and ^{36}Cl are now widely used for dating of bedrock surfaces [8–11], this method has seen limited use in depositional environments. Phillips and co-workers [3,8] have used ^{36}Cl to date large boulders on moraines and associated outwash terraces. We argue that a significant source of uncertainty in this and all other depositional systems arises from the accumulation of nuclides in the sampled clasts prior to deposition (i.e. 'inheritance').

Previous studies on depositional surfaces, including our own work, have revealed significant scatter in the effective ages derived from individual clasts sampled from such surfaces. At issue is how to interpret this scatter. One possible source of scatter is post-depositional turbation of clasts within the deposit, resulting in a mean nuclide production rate that is lower than that of the surface. In this case the surface clast with the largest effective age would provide a lower bound on the age of the deposit. If the scatter reflects instead the stochastic nature of pre-depositional nuclide inheritance, the surface clast with the lowest effective age provides an upper bound on the age of the deposit. The resolution requires sampling of the subsurface and averaging over many clasts to deal with the stochastic nature of inheritance. If the deposit has been static since deposition, all clasts will have experienced post-depositional nuclide production rates determined only by their depth within the deposit. The mean concentration profile should be an exponential profile that asymptotically approaches the mean inheritance at depth. If there has been significant post-depositional stirring of clasts (bio-, pedo- or cryoturbation), this expected profile will be disrupted in some way.

We describe here an amalgamation technique which greatly reduces the effort required to determine mean cosmogenic nuclide concentrations of surfaces composed of many clasts with disparate exposure histories. Anderson et al. [15] outlined this method and presented preliminary results. In this paper we further illustrate the inheritance problem and our proposed dating method with a set of numerical simulations, and then employ the method to estimate the ages of the Fremont River terraces.

2. Description of Fremont River terraces

The Fremont River drains the basalt-capped Aquarius and Fish Lake plateaus and cuts through two monoclines, the Waterpocket Fold and Caineville Reef, before joining the Muddy River near Hanksville to form the Dirty Devil River, a tributary to the Colorado River (Fig. 1). Tills and outwash deposits found in the drainages skirting the Aquarius Plateau indicate that the Fremont has at times been glacier fed. The Blind Lake and Donkey Creek tills have been correlated to the Pinedale glaciation and the Carcass Creek to the Bull Lake glaciation, based on morphology and extent of the deposits and on the degree of weathering of the clasts [16]. We have focused on the reach near North and South Caineville Mesas (Fig. 2), 15–20 km east of Capitol Reef National Park.

Four terraces can be traced through the field area, ranging in elevation from 20 to 135 m above the modern floodplain [5,17]. Each terrace consists of a several meter thick gravel veneer capping a strath surface eroded into shale and sandstone bedrock. We have labeled them FR0–FR4 from lowest to highest (Fig. 2), FR0 referring to the modern floodplain. FR1 and FR4 exist within the field as isolated remnants, with maximum widths of a few tens of meters. We have designated sublevels of FR2 as FR2A-C, from lowest to highest. FR2A and FR3 are the most extensively preserved of the terraces.

No absolute dates for either the moraines or the fluvial terraces of the Fremont River exist. Howard [5,17] relied upon careful correlation of the terraces with the morainal sequence on Boulder Mountain (Fig. 1), correlating terrace FR2A (his 4A) with the Pinedale glaciation, and terrace FR3 (his FR3A) with

the Bull Lake glaciation. Recent dating of glacial deposits in the type localities adjacent to the Wind River Range, Wyoming, reveals that each glaciation consists of numerous advances [3,25]. Clearly, absolute dating is needed to unravel the timing within any particular system.

All of the Fremont terraces have in common a single layer of varnished clasts, forming an interlocking desert pavement surface capping a thin (< 10 cm) layer of nearly clast-free silt, probably reflecting eolian inflation of the surface. The silt layer caps several meters of river gravels and sands. The stratigraphy is consistent with that of a braided channel. The total gravel thickness varies from less than 2 to roughly 10 m. Where visible, the base of the deposit makes a relatively planar contact with underlying shale and sandstone bedrock.

Clasts range in diameter up to tens of centimeters. The deposits are dominated by locally derived sandstone and shale, quartzite and chalcedony from the Triassic Shinarump conglomerate (presently exposed 50 km upstream in Capitol Reef National Park), and basalts from lava flows that mantle Boulder Mountain and Fish Lake Plateau [18]. In our cosmogenic radionuclide dating we have used only the well preserved and ubiquitous quartzite clasts on these terraces. The sizes of the quartzite clasts are similar from terrace to terrace. Their extreme resistance to weathering minimizes the problem of erosional loss from the sampled clasts. Finally, as the age of the

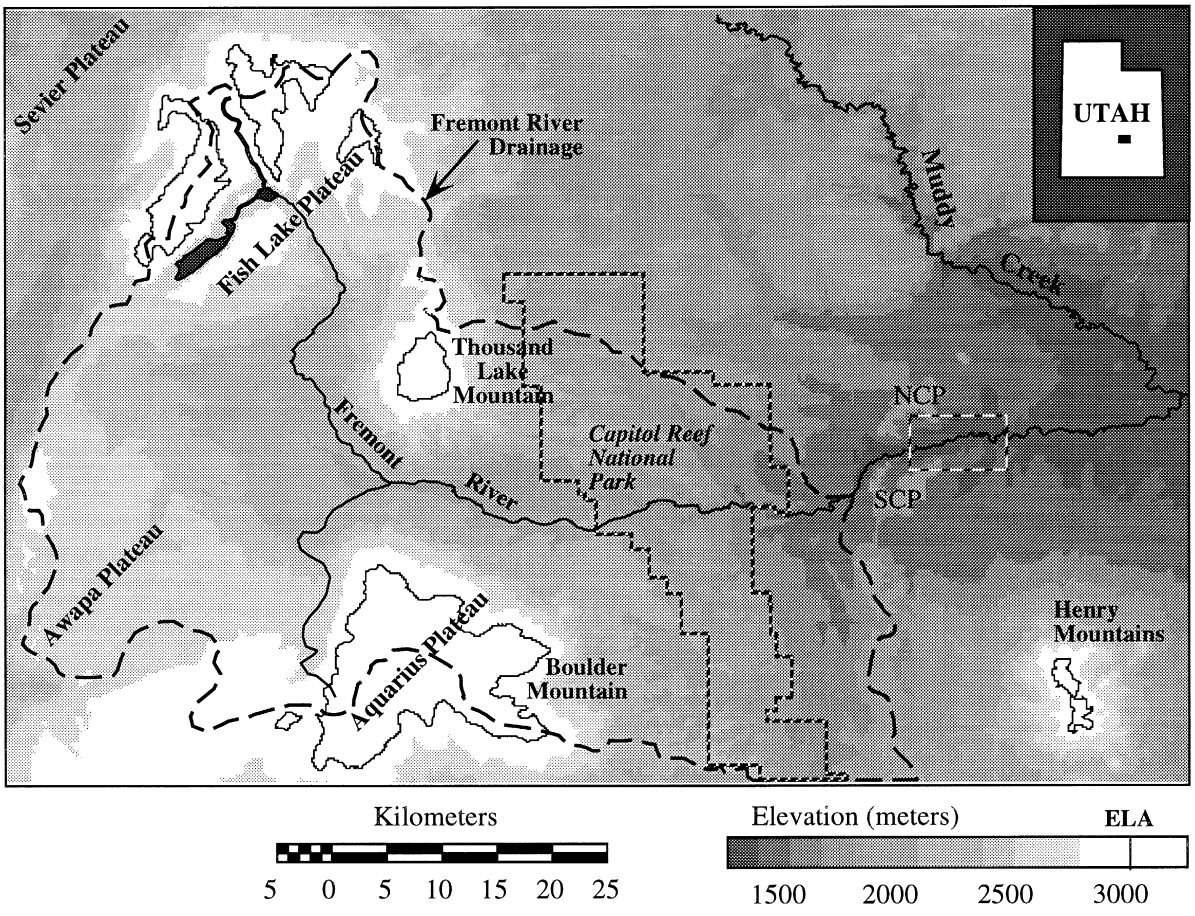

Fig. 1. Map of the Fremont River drainage upstream of the field area. Drainage area (dashed line) is just over 3700 km^2. The solid line surrounding the high plateaus represents the equilibrium line altitude (ELA) during the last glacial maximum, estimated to be 3170–3260 m [11]. The Caineville area within which the Fremont terraces are studied (Fig. 2) lies in the box east of Capitol Reef National Park.

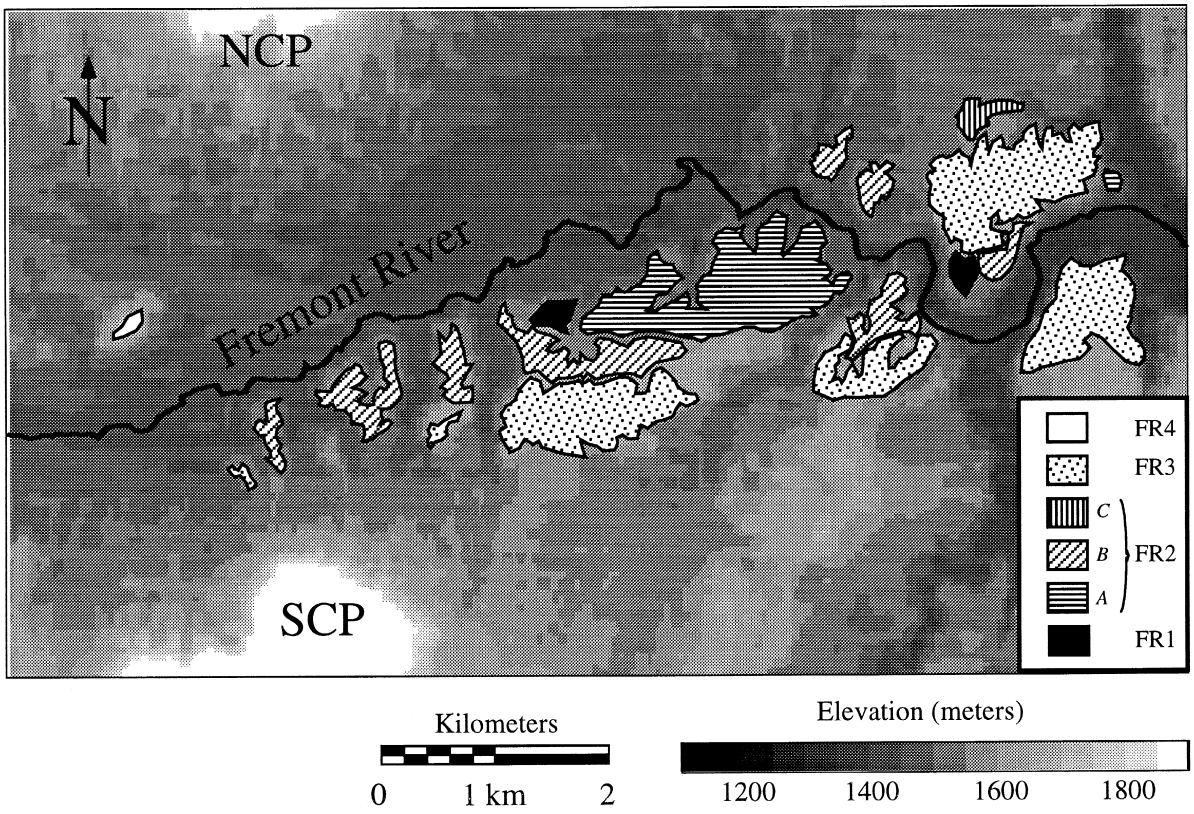

Fig. 2. Detailed topography adjacent to the Fremont River as it passes eastward through the gap between North Cainville Plateau (*NCP*) and South Caineville Plateau (*SCP*). The sampled terraces are depicted. Note the single small scraps of FR1 and FR4 surfaces, and the extensive preservation of FR2 and FR3 surfaces.

conglomerate from which they are derived is much greater than the half-lives of the radionuclides, we ignore inheritance from exposure in the ancient geomorphic system.

3. Numerical simulation of our technique

We present a numerical model of cosmogenic radionuclide accumulation histories for clasts within a hillslope/fluvial transport system that both illustrates the problem of constraining the terrace ages and provides a theoretical backdrop for our dating strategy.

Our model numerically integrates the differential equation for production and decay through time. Once the clasts are in the fluvial system, a series of three random numbers dictate how long the clast will spend within the system, whether it is in transport or storage at any time step, and its depth of burial if it is in storage. We specify that fluvial transport takes place only in short episodes during which the clast is at the surface; the rest of the time the clast is buried at a depth that is some fraction of a specified maximum. At the end of the transport cycle, clasts are instantaneously deposited on a terrace at some specified depth. Clasts deposited on the surface experience steady production, while clasts deposited beneath the surface experience production that decreases with time due to eolian inflation of the deposit [26]. At each time step, the model determines where the clast is within the system (on the hillslope, in the river, or on the final terrace), determines the clast depth and the associated cosmogenic radionuclide production rate, and updates the concentration.

This model incorporates several assumptions, some of which are applicable to most fluvial systems, while others should be considered specific to

the Fremont River: We assume a constant cosmic ray flux and therefore production rate. Cosmic ray irradiation is assumed to be negligible before hillslope exhumation brings the clast near the surface. We neglect variability in the hillslope exhumation process, assuming it to be spatially and temporally uniform within the catchment. We assume that topographic shielding from cosmic rays by snow and vegetation is insignificant.

3.1. Theoretical background

Cosmogenic nuclides are produced in situ from interactions between secondary cosmic ray particles and material at the earth's surface. Production decreases exponentially with depth:

$$P(z) = P_o e^{-z/z^*} \quad (1)$$

where $z^* = \Lambda/\rho$ is the *e*-folding length, or the ratio of the absorption mean-free path (Λ) of $\sim$145–160 g cm^{-2} and the material density (ρ) [20,21]. In quartz, which is an ideal mineral for measurement [9,10], ^{26}Al ($t_{1/2} = 0.705$ Ma) is produced primarily from silicon, while oxygen is the primary target for production of ^{10}Be ($t_{1/2} = 1.5$ Ma).

For exposure at a constant depth:

$$N(z,t) = N(z,0)e^{-\lambda t} + \frac{P_0}{\lambda} e^{-z/z^*}(1 - e^{-\lambda t}) \quad (2)$$

Here the first term represents the decay of the inherited concentration, N(z,0), while the second term represents the net increase in concentration due to production and subsequent decay.

The mean concentration of a cosmogenic nuclide at any particular depth, $\overline{N}$, is approximated by measuring 'amalgamated' samples consisting of equal mass aliquots of a large number of single clasts [15]. Eq. (2) may now be rewritten as an equation for the mean concentration. The difference in the concentration between two amalgamated samples, one from the surface and one from a known depth within the deposit, then reflects the expected difference in the deterministic post-depositional grow-in of cosmogenic radionuclides represented by the second term in Eq. (2). Ignoring decay, a full profile of the mean concentrations should reveal a simple shifted exponential:

$$\overline{N}(z) = \overline{N}_{in} + N_s e^{-z/z^*} \quad (3)$$

where $\overline{N}_{in}$ is the mean pre-depositional inheritance and N_s is the nuclide accumulation at the surface since deposition. This approximation is valid for times short relative to the decay time of the nuclide measured, and for shallow depths within which production by muons and by other less important mechanisms is negligible. Since there are two unknowns, N_{in} and N_s, two measurements suffice to solve the equation. Using this 'pairs technique' we can calculate the age of the surface:

$$\tau = \frac{1}{\lambda} \ln\left(\frac{\Delta P}{\Delta P - \lambda \Delta \overline{N}} \right) \quad (4)$$

where ΔP is the difference in production rates between the samples and $\Delta\overline{N}$ refers to the difference between the concentrations of the two samples. For young terraces, where decay may be neglected, this becomes $\tau = \Delta\overline{N}/\Delta P$.

In the case of a surface inflating by eolian deposition, the assumption of a constant production rate within the subsurface is incorrect. In this case our measured depth (z_s) overestimates the mean depth since deposition and thus underestimates the mean nuclide production rate for the subsurface sample. In addition, the production rate difference, ΔP, is a function of time. If we make the simplest assumption that silt thickness begins at zero and increases at a steady rate to its measured depth of L at the time of sampling, the correction factor $R = \overline{P}/P(z_s)$ for the mean production rate for the subsurface sample is:

$$R(L) = \frac{z^*}{L}\left[e^{L/z^*} - 1\right] \quad (5)$$

Eq. (4) should therefore be calculated with the difference in production rate of $\Delta P = P_0 - \frac{P(z_s)z^*}{L} \times [e^{L/z^*} - 1]$. While this correction can become large (of the order of 30% for a silt thickness $L = 0.5\ z^*$), the 10 cm thick silt caps of the Fremont River terraces (and $z^* = 80$ cm) result in only a 6% increase of the age estimate.

3.2. Model results

Fig. 3 illustrates the stochastic nature of the inheritance problem, showing simulated ^{10}Be concentration histories for a large number of clasts for two end-member scenarios. The terrace age was prescribed to be 100 ka, the surface production rate

$P_0 = 6$ atom/gm/yr. In Fig. 3A, the exhumation rate is 500 μm/yr, the maximum fluvial transport time is 200 ka, and the post-depositional eolian inflation rate is 10^{-3} m/ka. In Fig. 3B the exhumation rate varies randomly among the clasts, ranging from 17.5 to 42.5 μm/yr, while fluvial transport is zero, and the eolian inflation rate is zero. The large spread in the final concentrations of each group reflects the stochastic nature of the pre-depositional geomorphic processes. In the top run, Fig. 3A, the age estimated using Eq. (4) is 113 ka, reasonably close to the prescribed 100 ka age of the surface. The inset in Fig. 3B shows the dependence of the age estimate on the number of clasts used in the amalga-

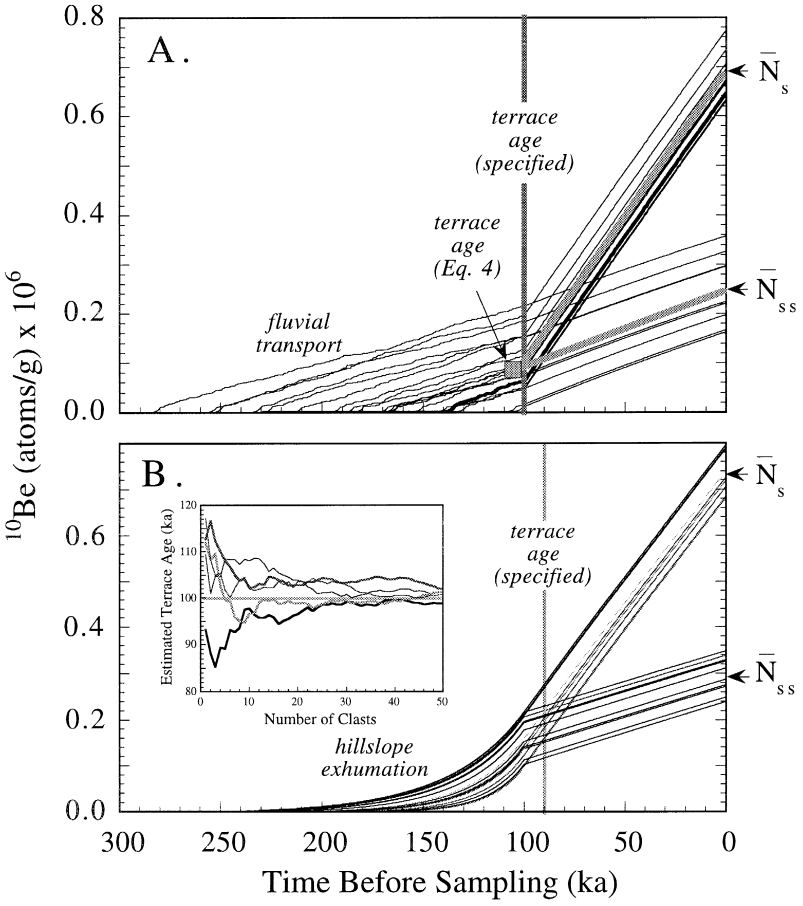

Fig. 3. Simulated ^{10}Be concentration histories of many clasts from hillslope exhumation through fluvial transport to terrace deposition. A steady sea level surface ^{10}Be production rate of $P_0 = 6$ atoms/gm/yr is assumed. At the final site of deposition, half of the clasts are deposited in the subsurface at an original depth of 1.0 m, the other half are deposited on the surface. The terrace age is ascribed to 100 ka. (A) Fluvial inheritance dominates. Twenty-four clast histories are shown. Exhumation of all clasts on hillslopes is rapid (500 μm/yr). Clasts spend a random time between 0 and 200 ka in fluvial transport. Eolian silt inflates the terrace surface by 0.1 m over 100 ka. An age estimate for the terrace of 113 ± 21 ka is obtained using the mean concentrations of $\bar{N}_s = 0.68 \pm 0.10$ and $\bar{N}_{ss} = 0.25 \pm 0.12 \times 10^6$ atom/gm and Eq. (4) (illustrated as the intersection of gray lines back-tracking concentration histories from mean concentrations). (B) Hillslope exhumation dominates inheritance. Twenty clast histories are shown. Exhumation rate is chosen randomly from between 17.5 and 42.5 μm/yr. Transport time within the fluvial system is negligible. The mean concentrations of the 10 surface clasts ($\bar{N}_s$) and of the 10 subsurface clasts ($\bar{N}_{ss}$ are shown, from which $\Delta\bar{N}$ is calculated. Inset depicts dependence of such age estimates on the number of clasts used in estimating the surface and subsurface mean concentrations, shown for 5 separate runs of 100 total clasts each (50 each in surface and subsurface).

mated samples. The age estimate improves as more and more clasts are amalgamated.

In Fig. 4 we depict similar simulations for four hypothetical terraces (A–D) whose height above the floodplain is dictated by a linear incision rate of 1.2 m/ka. We show the effective individual clast ages (N/P_0), as well as the effective mean age, for all surface clasts on each terrace. We then use Eq. (4) to estimate a true surface age for each terrace, using 30 randomly selected clasts both from this surface population and from the corresponding subsurface population at 1 m depth. The ages are depicted by the circles. It should be obvious that the mean concentration obtained from a single amalgamated sample of surface clasts would over-estimate the age of the surface. If all of the assumptions made in our model are correct, then Eq. (4) yields a reasonable approximation for the age of the surface. Correction of Eq. (4) for steady eolian inflation (with $L = 10$ cm) increases the age estimate by roughly 6%.

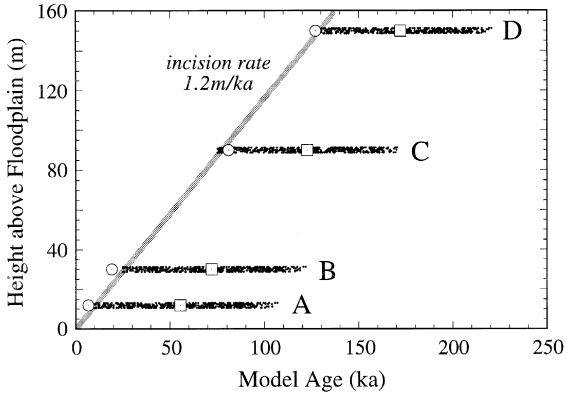

Fig. 4. Results of numerical simulations, resulting in calculated ^{10}Be ages for 2000 clasts from four hypothetical terraces in a system in which a linear incision rate (1.2 mm/yr; gray line) is imposed. The cloud of points at each elevation represents the wide spread of clast concentrations converted to effective ages through $\tau = N/P_0$, reflecting the variable inheritance of cosmogenic radionuclides during transport to the depositional site. Note that the youngest single clast age for each terrace is close to the specified age of the terrace (intersection of the gray line with that elevation). Boxes represent age estimates based upon samples amalgamated from 30 surface clasts selected at random from each of the four terraces. The large circles represent our model terrace age (Eq. (4)) using the pairs technique, based upon amalgamated surface and amalgamated subsurface samples. These model ages fall within 5% of the specified ages for each of the terraces.

3.3. Relative importance of exhumation and fluvial transport

Nuclide inheritance accrues during hillslope exhumation and fluvial transport. Ignoring for the moment the decay of the cosmogenic radionuclides, the inheritance during exhumation by steady surface lowering, $\dot{\epsilon}$, on hillslopes is the product of the surface production rate with the time it takes the sample to traverse the final production length scale z^* to the surface (e.g., [9]):

$$N_{hill} = \frac{P_0 z^*}{\dot{\epsilon}} \quad (6)$$

Variation in N_{hill} arises from several factors: (1) differences in surface production rates in the catchment due to altitudinal dependence of production rate; (2) variation in topographic shielding within the catchment, locally reducing the cosmic ray flux below that on an unshielded surface; and (3) variation in the local erosion rate in time and space.

Production within the fluvial system is complicated by the stochastic nature of the transport and burial processes. Clast depth, z(t), falls within the range [O,H], where O represents the surface and H is the depth of the gravel fill. Substituting $\beta = H/z^*$, the cosmogenic radionuclide accumulation history can be rewritten:

$$N_{fluvial} = P_0 T \int_0^{\beta z^*} \exp(-z/z^*)\,\Phi(z)\,dz \quad (7)$$

where T is the total transport time in the fluvial system and $\Phi(z)\,dz$ is the probability of finding the clast within the interval [z, z + dz] at any time. For the simplest case of uniform probability between the surface and depth H, the integral yields:

$$N_{fluvial} = P_0 T \left(\frac{1 - e^{-\beta}}{\beta} \right) \quad (8)$$

This reduces to the yet simpler expression $N_{fluvial} = P_0 T/\beta$ in thick deposits ($H > 2z^*$). As H increases the clast spends less time near the surface and accumulates fewer cosmogenic radionuclides. The simulated accumulation histories shown in Fig. 3A suggest that difference in total transport time is the principal factor in clast-to-clast variation in the fluvial component of nuclide inheritance. In addition, the mean rate of accumulation is significantly lower than the surface rate, P_0. The ratio of these mean

production rates, as deduced from the slopes in Fig. 3A, is roughly 4.6:1, meaning the effective production rate $P_{eff} = P_0/\beta$, with $\beta = 4.6$. Input parameters for the model were $H = 5$ m and $z^* = 0.8$ m; therefore the expected value of $\beta = H/z^*$ is 5.3. The simulation both illustrates and verifies this simple statistical treatment.

The relative contributions from hillslope and fluvial processes is the ratio of the effective times spent in the production zone in each of the geomorphic settings:

$$\frac{N_{fluvial}}{N_{hill}} = \frac{\dot{\epsilon} T(1 - e^{-\beta})}{\beta z^*} \approx \frac{\dot{\epsilon} T}{H} \quad (9)$$

When the exhumation rate is low and the transport time short, or the thickness of the floodplain storage system is great, the contributions from the hillslope system will dominate the inheritance signal, and vice versa. In the numerical simulations displayed in Fig. 3A ($\dot{\epsilon} = 0.5$ m/ka, $T_{max} = 200$ ka, and $H = 5$ m), for instance, the expected relative contributions to the inheritance should therefore be roughly 10:1 fluvial:hillslope. A more realistic estimate for the hillslope exhumation rate might be a few tens of microns per year, and the transport times in the fluvial system may not exceed several thousand years during times of high glacial discharge. Hillslope exhumation may therefore become an equal or dominant player in producing inheritance, the spread in single-clast cosmogenic radionuclide values reflecting nonuniformity in the erosion rates within the catchment.

4. Application to dating of the Fremont River terraces

4.1. Assumptions

We assume that the deposition rate of the terrace gravels is sufficiently rapid that there is no age structure within the deposit. There is no stratigraphic evidence for significant time spent during deposition of the terrace gravels, and rapid deposition is consistent with our interpretation of these gravels as braided stream deposits. We assume that the cosmogenic radionuclide inheritance signal is truly random. We assume that the mean inheritance of the clasts arriving on the surface can be characterized well by averaging the concentrations of a relatively small number of clasts (25–40). The number of clasts necessary to constrain the mean concentration well enough to extract the inheritance signal depends on the width of the distribution of clast inheritance. In addition, inheritance becomes a smaller portion of the total nuclide concentration on older terraces, making them more immune to the problems we are attempting to solve. We assume that there is no post-depositional 'stirring' of the terrace deposit. Finally, we assume that there has been no erosional loss from the horizontal portions of the terrace surfaces. This is consistent with the inflationary model of desert pavement formation [26].

4.2. Field methods

Samples were selected from the flattest surfaces, well away from terrace edges, in order to avoid areas subject to gravitational creep. Where possible, subsurface samples were obtained from pits dug in the interior of the terrace; otherwise they were from areas exposed by roadcuts. The location and elevation of each sample was noted. Topographic shielding was determined by measuring the vertical angle to the horizon measured in eight directions. We collected 30–70 clasts for amalgamation of surface and subsurface samples. On FR2 and FR3 we collected additional samples every 0.4–0.5 m, to a depth of 1.5–2.0 m, to obtain the concentration profiles. Clast sizes ranged from 5 cm to 20 cm.

4.3. Estimation of production rates

We have used the long-term average high latitude sea level production rate of 5.8 atom/gm/yr suggested in the most recent work of Nishiizumi et al. [24]. This is approximately 13% higher than that of Clark et al. [23] and 4% lower than the that of Nishiizumi [22]. The surface production rate for the given latitude and altitude is then adjusted using coefficients reported in Lal [9]. Variations in magnetic field strength introduce uncertainties into production rate estimates. Our calculations include a production rate uncertainty of 10%. The topographic shielding factor [22] was very near 1.0 in all cases. The soil density was estimated using a measured

Table 1
^{10}Be and ^{26}Al data: single clasts

Sample	Terrace	No. of clasts	Latitude	Altitude (km)	Depth (cm)	P^{10}Be	P^{26}Al	[Be] (ppm)	[Al] (ppm)	^{10}Be concentration (atom/μgm)	^{26}Al concentration (atom/μgm)	^{10}Be model age (ka)	^{26}Al model age (ka)
3294-1A	flood plain	1	38.3	1.42	0	16.9	103	25.0 ± 0.3	487 ± 29	0.105 ± 0.018	0.653 ± 0.081	6.2 ± 1.3	6.4 ± 1.0
3314-1A	flood plain	1	38.4	1.36	0	16.2	99	24.7 ± 0.3	234 ± 31	0.289 ± 0.025	1.744 ± 0.244	17.9 ± 2.4	17.8 ± 3.1
3314-1C	flood plain	1	38.4	1.36	0	16.2	99	25.8 ± 0.3	331 ± 16	0.323 ± 0.028	1.600 ± 0.107	20.0 ± 2.7	16.3 ± 2.0
9234-2.1	FR1	1	38.4	1.38	0	16.4	100	25.7 ± 0.3	71 ± 19	1.985 ± 0.058	11.283 ± 3.116	124.8 ± 13.4	119.8 ± 37.4
9234-2.2	FR1	1	38.4	1.38	0	16.4	100	25.2 ± 0.3	70 ± 19	1.707 ± 0.045	9.937 ± 2.769	106.8 ± 11.3	104.8 ± 32.7
9234-2.3	FR1	1	38.4	1.38	0	16.4	100	25.2 ± 0.3	105 ± 22	0.847 ± 0.035	4.957 ± 1.039	52.4 ± 5.7	50.9 ± 12.1
9234-2.8	FR1	1	38.4	1.38	0	16.4	100	24.1 ± 0.3	62 ± 20	0.390 ± 0.015	2.343 ± 0.745	24.0 ± 2.6	23.7 ± 8.0
9234-2.13	FR1	1	38.4	1.38	0	16.4	100	24.8 ± 0.3	295 ± 32	0.747 ± 0.047	3.851 ± 0.442	46.1 ± 5.5	39.3 ± 6.1
3314-2A	FR2A	1	38.4	1.40	0	16.6	101	25.1 ± 0.3	211 ± 12	1.056 ± 0.034	6.438 ± 0.427	64.4 ± 6.9	65.5 ± 8.1
3314-3A	FR2B	1	38.4	1.41	0	16.8	102	25.1 ± 0.3	229 ± 32	1.002 ± 0.052	6.578 ± 0.962	60.4 ± 6.9	66.3 ± 12.1
9053-4	FR2B	1	38.3	1.41	0	16.7	102	23.4 ± 0.3	113 ± 25	1.130 ± 0.043	6.805 ± 1.511	68.6 ± 7.5	69.0 ± 9.9
6202-2E	FR2C	1	38.4	1.42	0	16.9	103	16.9 ± 0.2	77 ± 22	1.416 ± 0.080	8.587 ± 2.572	85.3 ± 10.0	86.8 ± 28.6
9172-5B	FR2C	1	38.3	1.42	0	16.9	103	25.0 ± 0.3	244 ± 36	1.311 ± 0.057	7.875 ± 1.195	79.0 ± 8.8	79.5 ± 15.0
9244-7.1	FR2C	1	38.4	1.42	0	16.9	103	25.0 ± 0.3	184 ± 19	0.941 ± 0.050	6.016 ± 0.677	56.3 ± 6.5	60.0 ± 9.3
9244-7.2	FR2C	1	38.4	1.42	0	16.9	103	24.4 ± 0.3	344 ± 27	1.167 ± 0.037	7.186 ± 0.629	70.1 ± 7.5	72.1 ± 9.9
9244-7.3	FR2C	1	38.4	1.42	0	16.9	103	24.8 ± 0.3	207 ± 20	1.561 ± 0.041	10.469 ± 1.069	94.2 ± 10.0	106.9 ± 16.1
9244-7.5	FR2C	1	38.4	1.42	0	16.9	103	24.9 ± 0.3	260 ± 20	1.352 ± 0.037	8.641 ± 0.748	81.4 ± 8.6	87.4 ± 12.1
9244-7.6	FR2C	1	38.4	1.42	0	16.9	103	26.5 ± 0.3	442 ± 21	2.135 ± 0.072	10.418 ± 0.633	129.9 ± 14.1	106.3 ± 13.1
9073-4	FR3	1	38.4	1.44	0	17.2	105	22.7 ± 0.3	216 ± 45	2.020 ± 0.045	13.219 ± 2.766	121.1 ± 12.8	134.9 ± 33.5
9073-5	FR3	1	38.4	1.44	0	17.2	105	24.3 ± 0.3	363 ± 37	3.306 ± 0.058	21.841 ± 2.321	201.8 ± 21.5	233.6 ± 38.3
4155-1.1	FR3	1	38.4	1.44	0	17.1	104	41.4 ± 0.4		1.409 ± 0.060		84.0 ± 9.3	
4155-1.3	FR3	1	38.4	1.44	0	17.1	104	25.3 ± 0.3		2.638 ± 0.102		159.9 ± 17.8	
4155-1.6	FR3	1	38.4	1.44	0	17.1	104	65.5 ± 0.7		1.658 ± 0.107		99.1 ± 12.1	
4155-1.7	FR3	1	38.4	1.43	0	17.1	104	170.5 ± 1.8		1.401 ± 0.160		83.5 ± 12.9	

Altitudes and latitudes for samples were determined using: hand held GPS; laser EDM; triangulation with compass and topographic maps; and a combination of the three. Production as a function of latitude and altitude is calculated from equations given by Lal [9] and calibrations of Nishiizumi et al. [24]. The surface production rate is then adjusted to account for the depth to the subsurface samples: we estimate the terrace gravels to contain 30% large clasts, and the porosity of the matrix to be 35%, to arrive at a density of 2.1 ± 0.1 g/cm^3; we then calculate P(z) using Eq. (1) and Brown et al.'s [20] values of $\Lambda_{Be} = 145$ g/cm^2 (±5%) and $\Lambda_{Al} = 156$ g/cm^2 (±8%). Errors were propagated using the uncertainties given, with a 10% uncertainty assigned to the surface production rate and 7% to the sample depth. All samples were measured at the CAMS facility at Lawrence Livermore National Laboratory. Aluminum samples were normalized to standards prepared by Nishiizumi, KNSTD9860 (26Al:27Al = 9.86E − 12) and KNSTD9919 (26Al:27Al = 9.92E − 12). Aluminum blank ratios were uniformly less than 1.0E − 14. Beryllium samples were normalized to LLNL STD10000 (10Be:9Be = 1E11). Beryllium blank corrections take into account interference by the isobar ^{10}B and were uniformly less than 6.0E − 14.

30% clasts in the terrace deposit, and an estimated porosity of 0.35 within the fines, yielding a density of 2100 kg/m^3. We assume no vertical density structure, an assumption that results in negligible error.

4.4. Laboratory methods

Clasts were individually crushed and sieved to a uniform size of 200–500 μm, after which amalgamated samples, each representing a single depth, are constructed from equal mass aliquots of 25–40 individual clasts. Clean quartz separates were isolated by chemical leaching [28]. We added 0.5 mg of Be carrier to a 20 g sample of quartz and dissolved the sample in 3:1 HF:HNO_3. Aluminum concentrations were determined by atomic absorption spectroscopy on an aliquot of the dissolved sample. Al and Be were separated by ion chromatography and precipitated as metal hydroxides which were then oxidized to Al_2O_3 or BeO. The ratio of the radionuclide to the stable isotope was determined by accelerator mass spectrometry at Lawrence Livermore National Laboratory [29]. ^{10}Be concentrations were determined relative to an ICN standard and ^{26}Al to an NBS standard, both prepared by K. Nishiizumi. ^{10}Be/Be ratios were corrected for interference from ^{10}B. The measured ratios of both ^{10}Be and ^{26}Al were corrected for process blanks treated in the same way as the samples. The uncertainties quoted are the 1σ AMS errors only.

5. Results and discussion

5.1. Single clasts

The spread of effective ages derived from single clasts is very large (Table 1; Fig. 5A), demonstrating that the problem of inheritance is significant in this geomorphic system. In all cases, ^{26}Al and ^{10}Be results yield similar ages, implying that processing errors or long burial are not important. Even the cobbles sampled from the modern stream system show significant nuclide concentrations.

5.2. Amalgamated surface samples

Results from the surface amalgamated samples (numbers of clasts vary from 25–40; Table 2; Fig. 5B) show significantly less scatter than those for

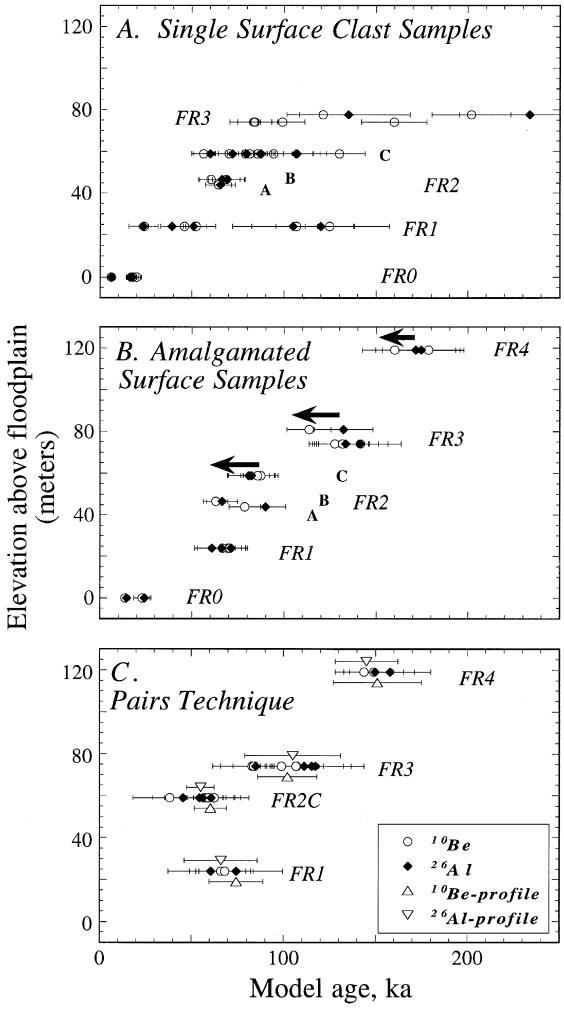

Fig. 5. Summary of results from ^{10}Be and ^{26}Al analyses of Fremont River terrace quartzite clasts (data shown in Table 1Table 2). ○ = ^{26}Al results; ◆ = ^{10}Be results. Ages were calculated using production rates determined using nuclear disintegration rates reported in Lal [9], and scaled to fit the production calibrations reported in Nishiizumi et al. [24]. (A) Results for whole single rock samples. Note the wide spread in effective ages. These are all maximum age estimates if the chief error is associated with inheritance. (B) Results for amalgamated surface samples representing at least 25 clasts. Note considerable reduction in age scatter from results from single clasts shown in (A). These ages correspond to the boxes in Fig. 4, and should be considered maximum ages. The length of the arrows show downward correction of mean ages from these amalgamated surface samples when inheritance is taken into account (see C). (C) Results of the pairs technique employing two amalgamated samples. Triangles represent the ^{26}Al and ^{10}Be model ages determined using the profile technique (see Fig. 4).

single clasts. Most repeat samples using different sets of clasts show some overlap, both in ^{26}Al and in ^{10}Be. If the spread in effective ages from single clasts represents variable inheritance, then age estimates from these surface amalgamated samples are to be considered maxima.

5.3. Paired–amalgamated sample technique

In Fig. 5C we plot age estimates of the terraces adjusted for inheritance (Eq. (4)). The model ages for the higher terraces increase with elevation, although the lowest terrace (FR1) appears to be slightly older than the next highest terrace. The arrows on Fig. 5B depict the downward shift in the age estimate when inheritance is taken into account.

5.4. Profile technique

Fig. 6 shows vertical concentration profiles of four terraces. Two of the terraces, FR2C and FR3, were sampled at several depths. The profile of FR2C consists of two amalgamated samples collected from the surface, one from 0.4 m, two from 0.6 m, and one from 1.0 m depth. The FR3 profile consists of four surface samples, one from 0.5 m, and two each from 1.0 and 1.5 m. The best-fitting shifted exponentials (Eq. (3)) fit the shapes of the full profiles quite well. For the higher surfaces, the shift representing pre-depositional inheritance is similar, about 24 ± 8 ka. The inheritance shift for FR1 is minimal. The age estimates based upon these profiles are shown as triangles on Fig. 5C.

At this location there is no well expressed terrace that corresponds to the last glacial maximum (LGM). The surface in the proper elevational range is FR1. The pairs technique suggests that FR1 is slightly older than FR2C, which is geomorphically impossible. It is likely that the gravel deposits on this small terrace remnant consist entirely of material quarried from the adjacent older terrace either at the end of the depositional phase, or during the post-depositional evolution of the scarp separating the two. This would result in an age estimate for FR1 similar to that determined for FR2C, which indeed is what we observe. An alternative explanation is that the LGM is represented here by the current floodplain (FR0). In either case, given the minor, narrow exposures in this reach of the Fremont River, we are not confident in our dating of FR1.

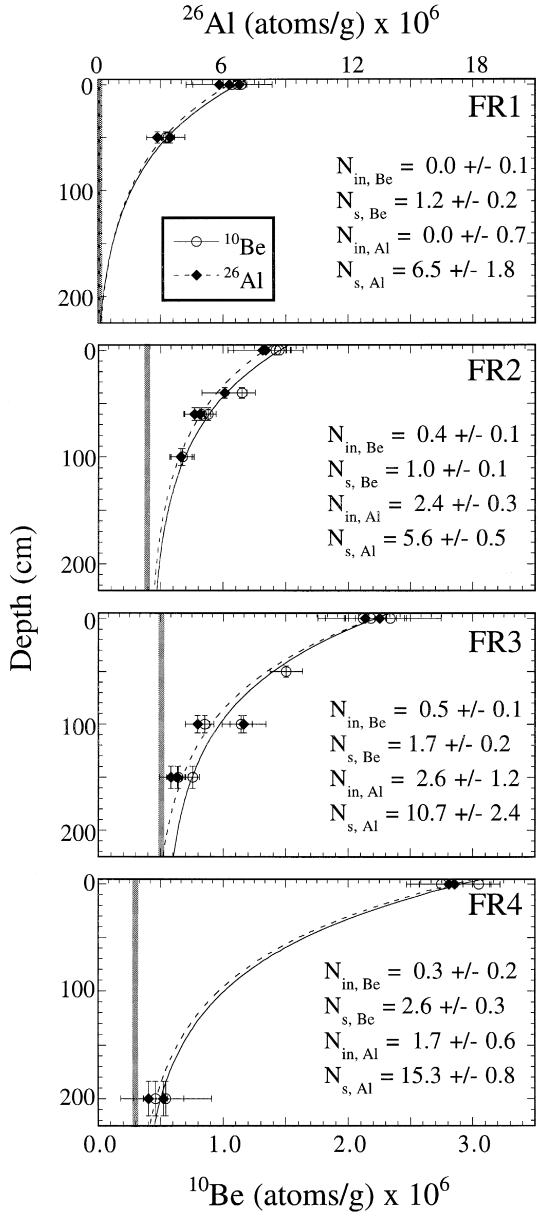

Fig. 6. Full cosmogenic radionuclide concentration profiles for FR2C and FR3, and the amalgamated sample results used in the pairs techniques on all terraces. Note ^{26}Al (top axis) and ^{10}Be (bottom axis) are plotted on scales that differ by a factor of 6.0. Curves are best fits to Eq. (3), with z^* fixed at 0.8 m (solid line ^{10}Be; dashed ^{26}Al). The gray vertical lines represent best fits for the inheritance, N_{in}, (width indicates error in estimate of inheritance) for FR2C, FR3 and FR4. Inheritance on FR1 appears to be minimal (see text for discussion). The best fit for the post-depositional component of the radionuclide concentration at the surface, N_s, is then used to estimate the age of the surface.

Table 2
^{10}Be and ^{26}Al data: amalgamated samples

Sample	Terrace	No. of clasts	Latitude	Altitude (km)	Depth (cm)	P^{10}Be	P^{26}Al	[Be] (ppm)	[Al] (ppm)	^{10}Be concentration (atom/μgm)	^{26}Al concentration (atom/μgm)	^{10}Be model age (ka)	^{26}Al model age (ka)
3294-1B	flood plain	30	38.3	1.42	0	16.9	103	28.0 ± 0.3	146 ± 7	0.388 ± 0.071	2.47 ± 0.15	23.1 ± 4.8	24.3 ± 2.9
3314-1B	flood plain	30	38.4	1.36	0	16.2	99	25.9 ± 0.3	222 ± 11	0.219 ± 0.023	1.41 ± 0.09	13.6 ± 2.0	14.4 ± 1.7
9234-2A	FR1	30	38.4	1.38	0	16.4	100	25.3 ± 0.3	145 ± 23	1.119 ± 0.036	6.39 ± 1.04	69.5 ± 7.4	66.2 ± 13.1
9234-2B	FR1	30	38.4	1.38	0	16.4	100	25.2 ± 0.3	276 ± 28	1.073 ± 0.035	5.90 ± 0.64	66.5 ± 7.1	60.9 ± 9.3
9234-2C	FR1	32	38.4	1.38	0	16.4	100	25.0 ± 0.3	508 ± 28	1.143 ± 0.070	6.87 ± 0.49	70.9 ± 8.5	71.3 ± 9.1
9234-6A	FR1	30	38.4	1.38	50	7.9	51	24.9 ± 0.3	346 ± 31	0.563 ± 0.026	3.52 ± 0.36	66.1 ± 16.5	60.6 ± 23.1 *
9234-6B	FR1	30	38.4	1.38	50	7.9	51	24.5 ± 0.3	346 ± 28	0.546 ± 0.025	2.89 ± 0.26	68.2 ± 17.0	74.4 ± 25.2 *
3314-2B	FR2A	36	38.4	1.39	0	16.6	101	24.9 ± 0.3	150 ± 8	1.285 ± 0.041	8.72 ± 0.51	78.6 ± 8.4	89.8 ± 10.9
3314-3B	FR2B	31	38.4	1.40	0	16.8	102	25.3 ± 0.3	177 ± 10	1.043 ± 0.034	6.58 ± 0.45	62.9 ± 6.7	66.4 ± 8.3
9244-7A	FR2C	30	38.4	1.41	0	16.9	103	25.2 ± 0.3	201 ± 22	1.448 ± 0.044	8.16 ± 0.92	87.2 ± 9.3	82.3 ± 12.9
9244-7B	FR2C	30	38.4	1.41	0	16.9	103	25.3 ± 0.3	253 ± 20	1.420 ± 0.044	8.02 ± 0.70	85.5 ± 9.1	80.8 ± 11.1
4175-2A	FR2C	33	38.3	1.41	40	9.5	60	24.8 ± 0.3	215 ± 18	1.149 ± 0.054	6.16 ± 0.55	38.5 ± 14.2	45.6 ± 27.3 *
9244-8A	FR2C	25	38.4	1.41	60	7.1	46	25.4 ± 0.3	653 ± 44	0.828 ± 0.035	4.96 ± 0.39	62.5 ± 13.8	56.2 ± 20.6 *
9244-8B	FR2C	25	38.4	1.41	60	7.1	46	23.9 ± 0.3	738 ± 20	0.879 ± 0.032	4.71 ± 0.25	57.2 ± 12.7	60.8 ± 20.5 *
4175-3A	FR2C	35	38.3	1.41	100	4.0	27	24.4 ± 0.3	459 ± 18	0.676 ± 0.046	4.04 ± 0.27	59.3 ± 9.9	54.4 ± 14.4 *
3314-4B	FR3	32	38.4	1.44	0	17.2	105	24.7 ± 0.3	251 ± 12	1.898 ± 0.050	12.99 ± 0.68	113.4 ± 12.0	132.2 ± 16.0
9244-9A	FR3	37	38.3	1.44	0	17.1	104	24.8 ± 0.3	150 ± 16	2.338 ± 0.063	13.72 ± 1.51	141.4 ± 15.1	141.1 ± 22.5
9244-9B	FR3	34	38.3	1.44	0	17.1	104	25.3 ± 0.3	204 ± 14	2.182 ± 0.063	13.01 ± 0.97	131.7 ± 14.1	133.3 ± 17.8
4155-1A	FR3	32	38.4	1.44	0	17.1	104	53.0 ± 0.6		2.182 ± 0.102		131.4 ± 14.9	
4155-1B	FR3	32	38.4	1.44	0	17.1	104	54.2 ± 0.6		2.119 ± 0.076		127.5 ± 13.9	
4155-2A	FR3	40	38.4	1.44	50	8.3	53	36.6 ± 0.4		1.509 ± 0.065		83.0 ± 22.1	*
4155-3A	FR3	30	38.4	1.43	100	4.0	27	25.6 ± 0.3	335 ± 22	1.144 ± 0.044	7.10 ± 0.53	83.9 ± 13.7	85.0 ± 23.3 *
4155-3B	FR3	23	38.4	1.43	100	4.0	27	25.1 ± 0.3	575 ± 27	0.853 ± 0.036	4.85 ± 0.30	107.2 ± 16.7	117.3 ± 26.4 *
4155-4A	FR3	40	38.4	1.43	150	1.9	14	25.3 ± 0.3	522 ± 27	0.756 ± 0.027	3.88 ± 0.26	98.9 ± 12.8	111.2 ± 21.3 *
4155-4B	FR3	40	38.4	1.43	150	1.9	14	25.2 ± 0.3	446 ± 27	0.643 ± 0.026	3.56 ± 0.28	106.7 ± 13.7	115.1 ± 21.7 *
9234-3A	FR4	45	38.3	1.49	0	17.8	109	25.5 ± 0.3	371 ± 15	2.747 ± 0.088	17.40 ± 0.86	160.1 ± 17.5	174.4 ± 21.2
9234-3B	FR4	37	38.3	1.49	0	17.8	109	25.4 ± 0.3	338 ± 17	3.048 ± 0.086	17.12 ± 1.03	178.4 ± 19.3	171.4 ± 21.8
9234-4A	FR4	45	38.3	1.49	200	1.0	7	26.5 ± 0.3	103 ± 15	0.460 ± 0.048	2.47 ± 0.37	149.1 ± 17.7	158.0 ± 23.4 *
9234-4B	FR4	45	38.3	1.49	200	1.0	7	47.7 ± 0.5	214 ± 31	0.544 ± 0.082	3.20 ± 0.50	143.8 ± 25.9	149.6 ± 23.7 *

Altitudes and latitudes for samples were determined using: handheld GPS; laser EDM; triangulation with compass and topographic maps; and a combination of the three. Production as a function of latitude and altitude is calculated from equations given by Lal [9] and calibrations of Nishiizumi et al. [24]. The surface production rate is then adjusted to account for the depth to the subsurface samples: we estimate the terrace gravels to contain 30% large clasts, and the porosity of the matrix to be 35%, to arrive at a density of 2.1 ± 0.1 g/cm^3; we then calculate P(z) using Eq. (1) and Brown et al.'s [20] values of $\Lambda_{Be} = 145$ g/cm^2 ($\pm 5\%$) and $\Lambda_{Al} = 156$ g/cm^2 ($\pm 8\%$). Errors were propagated using the uncertainties given, with a 10% uncertainty assigned to the surface production rate and 7% to the sample depth. The model ages given for subsurface samples (labeled with a *) are calculated with Eq. (4), using the mean surface production rate and concentration for that terrace. All samples were measured at the CAMS facility at Lawrence Livermore National Laboratory. Aluminum samples were normalized to standards prepared by Nishiizumi, KNSTD9860 (26Al:27Al = 9.86E − 12) and KNSTD9919 (26Al:27Al = 9.92E − 12). Aluminum blank ratios were uniformly less than 1.0E − 14. Beryllium samples were normalized to LLNL STD10000 (10Be:9Be = 1E11). Beryllium blank corrections take into account interference by the isobar ^{10}B and were uniformly less than 6.0E − 14.

The profiles and amalgamated sample pairs suggest ^{10}Be-based age estimates of 60 ± 9 ka for FR2C, 102 ± 16 ka for FR3, and 151 ± 24 ka for FR4. While the uncertainties are large, comparison with the global ice volume record depicted by the δ^{18}O curve [30] supports the idea that the Fremont terraces were emplaced in late glacial or glacial maximum times (Fig. 7). The amalgamated surface sample results (Fig. 5B) from the FR2A and FR2B surfaces imply that they may be roughly coeval with the FR2C surface. In the absence of samples from depth on these two extensive lower surfaces, we cannot further constrain the time span that these three surfaces represent. If they are all associated with isotope stage 4, then the vertical range of depositional surfaces produced during this glacial stage was roughly 30 m.

We note that the 102 ka age for the FR3 terrace corresponds well with recently reported ages for the WR3 terrace along the Wind River. The Wind River has 15 well preserved terraces [14] and displays a rich response to small fluctuations in the global ice volume record. The Pinedale moraine and associated terrace sequence includes last glacial maximum dates ranging from 17 to 21 ka. The Bull Lake glaciation includes a wide temporal range of morainal and terrace features. The associated WR3 terrace has been dated, using ^{36}Cl, at 126–103 ka [19]. Results of work using ^{10}Be methods parallel to our own implies an age of roughly 100 ka for this terrace [25]. While the age the FR2C terrace does not correlate with any dated surface in the Wind River sequence, the Sierran system does record such an event (Younger Tahoe in the Bloody Canyon moraines: 40–55 ka [13]).

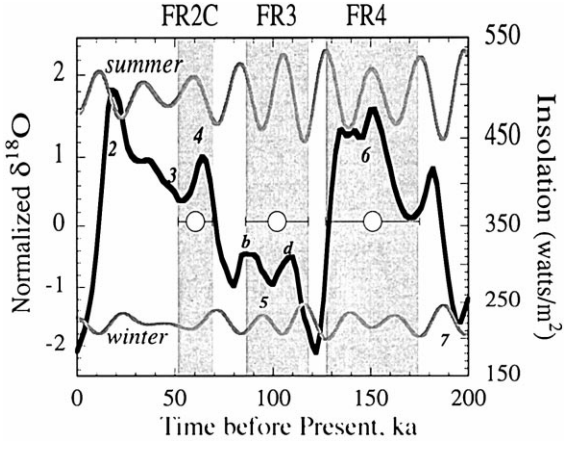

Fig. 7. Age estimates of the three best dated terraces (FR2C, FR3, and FR4) shown against the last 250 ka of the normalized global δ^{18}O record (the scale on the left axis is standard deviations about the mean) [27]; oxygen-isotope stages are numbered. The terrace ages (gray bars) were determined using production rates scaled by the Nishiizumi et al. [24] calibrations, and post-depositional accumulations of cosmogenic radionuclides constrained by fitting the concentration profiles shown in Fig. 6. Also shown are the summer and winter insolation calculations of Berger and Loutre [31] for 30°N. The terrace ages correspond roughly to global ice volume maxima in stages 4, 5d and 6, and to maxima in the summer insolation and minima in the winter insolation histories.

Knowledge of the ages of these terraces allows us to estimate various geomorphic process rates within the Fremont River system. While the incision rate of the river varies with time (as the existence of terraces attests), even the mean incision rate between times of terrace abandonment appears to vary widely. The terrace ages suggest variation by roughly a factor of 3, from 0.30 to 0.85 m/ka around a mean of 0.6 m/ka. We therefore caution against placing much faith in linear interpolation or extrapolation of terrace ages from any pair of known ages, as is commonly done.

The inheritance, $\overline{N}_{in}$, is of the same order for all three terraces (0.42×10^6 atom/g ^{10}Be for FR2C, 0.48×10^6 atom/g for FR3, and 0.44×10^6 atom/g for FR4). This corresponds to the arrival of clasts at the terrace with mean effective exposure ages of 30–40 ka. The inheritance can be used to constrain hillslope exhumation rates and fluvial transport times. If we assume rapid fluvial transport ($\overline{N}_{in} = \overline{N}_{hill}$), we can solve Eq. (6) for the mean hillslope erosion rate to yield $\dot{\epsilon} = 30$ m/Ma. If we assume exhumation to be rapid (i. e., $\overline{N}_{in} = \overline{N}_{fluvial}$, then $N_{fluvial}$ corresponds to a mean transport time of 166 ka (using Eq. (8) with $H = 5$ m). Because inheritance is the sum of these two processes, the exhumation determined here is a minimum and the fluvial transport time is a maximum. Given the 40–50 km distance from our source area to our sampled terraces transport times of the order 10^5 yr seem unreasonable. The 30 m/Ma erosion rate, on the other hand, is similar to bedrock erosion rates measured elsewhere in the arid American west [12,1]. This argues that the primary source of inheritance in the Fremont system is obtained during exhumation on hillslopes within the headwa-

ters, and that clast-to-clast variability in inheritance is due to high variability in local rates of exhumation. That the mean inheritance is roughly consistent from terrace to terrace could be interpreted as signifying that the mean weathering rate within the basin over this interval of time has been surprisingly constant.

6. Conclusions

The large spread of single clast ages implies a wide scatter in the inheritance signal, raising a cautionary flag against the use of small numbers of clasts in dating depositional terraces. This scatter can be reduced significantly by using samples consisting of aliquots from large numbers of clasts. The reproducibility of the concentration values from samples amalgamated from 25–40 clasts implies that these are sufficient numbers to constrain the mean concentrations in this particular geomorphic system.

Using the latest Nishiizumi et al. production rates, we estimate ^{10}Be ages of roughly 60 ± 9, 102 ± 16 and 151 ± 24 ka for three of the terraces along the Fremont River. These ages are consistent with a terrace genesis model wherein terrace gravels are laid down in braided outwash plains associated with high water and sediment flux during glacial maxima, and are abandoned as the Fremont River begins to incise due to high water and low sediment flux upon retreat of the glaciers [2,6]. Our dating implies that climate swings that generate only small and short-lived variations in global ice volume are sufficient to generate significant glacial systems in small mountain chains. The incision rate between terrace-forming events appears to vary by a factor of three, implying that the method of dating strath terraces by fitting them to a single, long-term mean incision rate yields at best a crude approximation.

At this point, one must still exercise considerable geological experience in the interpretation of cosmogenic radionuclide dates from these depositional terraces. By developing a strategy to account for the geomorphic delivery system of clasts to the final site of deposition, we have dealt with a large portion of the noise in the system. The profile technique, employed here on two of the terraces, generates the expected inheritance-shifted exponential profile, supporting the use of the pairs technique in this system for determining both the age and inheritance. We suggest that this is probably not a general result, and that full concentration profiles should be used to test for problems related to post-depositional turbation of clasts and for inflation or deflation of the surface within any system being dated. The inheritance of cosmogenic radionuclides is significant and must be taken into account in estimating ages of depositional surfaces. Studies of the rate of pedogenesis, and of the rate of weathering of clasts on these terraces can now proceed with the knowledge that the timing has been established to within roughly 10–20%, most of this error being in choice of cosmogenic production rate.

Acknowledgements

We gratefully acknowledge the Petroleum Research Fund of the American Chemical Society, a grant from the Center for Accelerator Mass Spectrometry at Lawrence Livermore National Laboratory, and a Cole award from the Geological Society of America, for support of this research. We thank the following individuals for their help in the field, the lab, and/or for reviewing early versions of this paper: Christian Brauderick, Alex Densmore, Greg Dick, James Georgis, Joe Koning, Craig Lundstrom, Greg Pratt, Eric Small, and Melissa Swartz. In addition, thorough and constructive reviews of an earlier version of the manuscript by K. Nishiizumi, E. Brown and an anonymous reviewer aided significantly in its condensation. This work was partially supported under the auspices of the DOE by LLNL under contract W-7405-Eng-48. *[MK]*

References

[1] E.E. Small, R.S. Anderson, R.C. Finkel, ^{10}Be and ^{26}Al erosion rates from summit flats in the Rocky Mountains: Constraints on the rate of relief production, EOS Trans. Am. Geophys. Union 76 (1995) 690.

[2] G.M. Richmond, Quaternary stratigraphy of the La Sal Mountains Utah, U.S. Geol. Surv. Prof. Pap. 324 (1962) 135.

[3] O.A. Chadwick, R.D. Hall, J. Conel, F.M. Phillips, M. Zreda, M.D. Gosse, Glacial deposits and river terraces, in: Wind River Basin, Friends of the Pleistocene Rocky Mountain Cell, Field Conference Guidebook, 1994, 141 pp.

[4] C. Jaworowski, A probable new Lava Creek ash locality: implications for Quaternary geologic studies in the western Wind River basin, Wyoming, USA, Friends of the Pleistocene Rocky Mountain Cell, Field Conference Guidebook, 1994, pp. 135–141.
[5] A.D. Howard, Study of process and history in desert landforms near the Henry Mountains, Utah, Ph.D. Thesis, Johns Hopkins Univ., Baltimore, MD, 1970, 198 pp.
[6] S. Sinnock, Glacial moraines, terraces and pediments of Grand Valley, western Colorado, New Mexico Geol. Soc. 32nd Field Conference Guidebook, 1981, pp. 113–120.
[7] J.L. Slate, W.B. Bull, T.L. Ku, M. Shafiquillah, D.J. Lynch, Yi-Pu Huang, Soil-carbonate genesis in the Pinacate Volcanic Field, northwestern Sonora, Mexico, Quat. Res. 35 (1991) 400–416.
[8] F. Phillips, M.G. Zreda, S.S. Smith, D. Elmore, P.W. Kubik, P. Sharma, Cosmogenic chlorine-36 chronology for glacial deposits at Bloody Canyon, eastern Sierra Nevada, Science 248 (4962) (1990) 1529–1532.
[9] D. Lal, Cosmic ray labeling of erosion surfaces: in situ nuclide production and erosion models, Earth Planet. Sci. Lett. 104 (1991) 424–439.
[10] K. Nishiizumi, C.P. Kohl, J.R. Arnold, R.I. Dorn, J. Klein, D. Fink, R. Middleton, D. Lal, Role of in situ cosmogenic nuclides ^{10}Be and ^{26}Al in the study of diverse geomorphic processes, Earth Surf. Process. 18 (1993) 407–425.
[11] P.R. Bierman, Using in situ produced cosmogenic isotopes to estimate rates of landscape evolution: A review from the geomorphic perspective, J. Geophys. Res. — Solid Earth 99 (1994) 13885–13896.
[12] P.R. Bierman, How fast do rocks erode? New answers from atom counting, Geol. Soc. Am. Abstr. with Programs 27 (1995) 44.
[13] F.M. Phillips, M.G. Zreda, L.V. Benson, M.A. Plummer, D. Elmore, P. Sharma, Chronology for fluctuations in late Pleistocene Sierra Nevada glaciers and lakes, Science 274 (1996) 749–751.
[14] O.A. Chadwick, R.D. Hall, F.M. Phillips, Pleistocene glaciations in the Rocky Mountains: Bull Lake and Sacagawea Ridge revisited, Geol. Soc. Am. Bull. (in press).
[15] R.S. Anderson, J.L. Repka, G.S. Dick, Explicit treatment of inheritance in dating depositional surfaces using in situ ^{10}Be and ^{26}Al, Geology 24 (1996) 47–51.
[16] R.F. Flint, C.S. Denny, Quaternary Geology of Boulder Mountain, Aquarius Plateau, Utah, U.S., Geol. Surv. Bull. 1061-D (1956) 103–164.
[17] A.D. Howard, Quaternary landform evolution of the Dirty Devil River system, Utah, Geol. Soc. Am. Abstr. with Programs 18 (1986) 641.
[18] G.H. Billingsly, P.W. Huntoon, W.J. Breed, Geologic map of Capitol Reef National Park and vicinity, Emery, Garfield, Millard and Wayne Counties, Utah, Utah Geological and Mineral Survey, Salt Lake City, 1987.
[19] F.M. Phillips, M.G. Zreda, J.C. Gosse, J. Klein, E.B. Evenson, R.D. Hall, O.A. Chadwick, P. Sharma, Cosmogenic ^{36}Cl and ^{10}Be ages of Quaternary Glacial and fluvial deposits of the Wind River Range, Wyoming, Geol. Soc. Am. Bull. (in press).
[20] E.T. Brown, E.J. Brook, G.M. Raisbeck, F. Yiou, M.D. Kurz, Effective attenuation lengths of cosmic rays producing ^{10}Be and ^{26}Al in quartz: Implications for exposure age dating, Geophys. Res. Lett. 19 (1992) 369–372.
[21] K. Nishiizumi, Cosmogenic production of ^{10}Be and ^{26}Al on the surface of the Earth and underground, Abstracts 8th Int. Conf. on Geochronology, Cosmochronology, and Isotope Geology, U.S. Geol. Surv. Circ. 1107 (1994) 234.
[22] K. Nishiizumi, Cosmic ray production rates of ^{10}Be and ^{26}Al in quartz from glacially polished rocks, J. Geophys. Res. 94 (1989) 17907–17915.
[23] D.H. Clark, P.R. Bierman, P. Larsen, Improving in situ cosmogenic chronometers, Quat. Res. 44 (1995) 367–377.
[24] K. Nishiizumi, R.C. Finkel, J. Klein, C.P. Kohl, Cosmogenic production of ^{7}Be and ^{10}Be in water targets, J. Geophys. Res. 101 (1996) 22225–22232.
[25] G.S. Dick, R.S. Anderson, J.L. Repka, O.A. Chadwick, R.C. Finkel, ^{10}Be and ^{26}Al dating of fluvial terraces, Wind River, Wyoming, EOS Trans. Am. Geophys. Union 76 (1995) 690.
[26] S.G. Wells, L.D. McFadden, J. Poths, C.T. Olinger, Cosmogenic ^{3}He surface-exposure dating of stone pavements — Implications for landscape evolution in deserts, Geology 23 (1995) 613–617.
[27] T.E. Cerling, H. Craig, Geomorphology and in-situ cosmogenic isotopes, Rev. Earth Planet. Sci. 22 (1994) 273–317.
[28] C.P. Kohl, K. Nishiizumi, Chemical isolation of quartz for measurement of in-situ-produced cosmogenic nuclides, Geochim. Cosmochim. Acta 56 (1992) 3583–3587.
[29] J.C. Davis, I.D. Proctor, J.R. Southon, M.W. Caffee, D.W. Heikkinen, M.L. Roberts, K.W. Moore, K.W. Turteltaub, D.E. Nelson, D.H. Loyd, J.S. Vogel, LLNL/UC AMS facility and research program, Nucl. Instrum. Methods Phys. Res. B 52 (1990) 269–272.
[30] J. Imbrie, J.D. Hays, D.G. Martinson, A. McIntyre, A.C. Mix, J.J. Morley, N.G. Pisias, W.L. Prell, N.J. Shackelton, The orbital theory of Pleistocene climate: support from a revised chronology of the marine δ^{18}O record, in: A. Berger, J. Imbrie, J. Hays, G. Kukla, B. Saltzman (Eds.), Milankovitch and Climate: Understanding the Response to Astronomical Forcing, Part 1, Reidel, Higham, MA, 1984, pp. 269–305.
[31] A. Berger, M.F. Loutre, Insolation values for the climate of the last 10 million of years, Quat. Sci. Rev. 10 (1991) 297–317.